

# Dynamics of a Nonequilibrium Discontinuous Quantum Phase Transition in a Spinor Bose-Einstein Condensate

Matthew T. Wheeler,<sup>1,3</sup> Hayder Salman,<sup>2,3</sup> and Magnus O. Borgh<sup>1,3</sup>

<sup>1</sup>*Physics, Faculty of Science, University of East Anglia, Norwich Research Park, Norwich, NR4 7TJ, UK*

<sup>2</sup>*School of Mathematics, University of East Anglia, Norwich Research Park, Norwich, NR4 7TJ, UK*

<sup>3</sup>*Centre for Photonics and Quantum Science, University of East Anglia, Norwich Research Park, Norwich, NR4 7TJ, UK*

Symmetry-breaking quantum phase transitions lead to the production of topological defects or domain walls in a wide range of physical systems. In second-order transitions, these exhibit universal scaling laws described by the Kibble-Zurek mechanism, but for first-order transitions a similarly universal approach is still lacking. Here we propose a spinor Bose-Einstein condensate as a testbed system where critical scaling behavior in a first-order quantum phase transition can be understood from generic properties. We generalize the Kibble-Zurek mechanism to determine the critical exponents for: (1) the onset of the decay of the metastable state on short times scales, and (2) the number of resulting phase-separated ferromagnetic domains at longer times, as a one-dimensional spin-1 condensate is ramped across a first-order quantum phase transition. The predictions are in excellent agreement with mean-field numerical simulations and provide a paradigm for studying the decay of metastable states in experimentally accessible systems.

## I. INTRODUCTION

Classical and quantum nonequilibrium phase transitions arise in many areas of physics, ranging from cosmology [1, 2], to condensed matter [3–8], and to ultracold atomic gases [9–12]. For a second-order (continuous) phase transition, a correlation length and time scale can be identified that characterise the coherence and dynamical response of the system. As the critical point is approached, both of these exhibit power-law divergences described by critical exponents [13, 14]. In nonequilibrium phase transitions, this implies that close to the critical point, the system is no longer able to adiabatically follow the ground state [15, 16]. Causally disconnected regions then choose the new broken symmetry state independently. This results in the formation of topological defects or domain boundaries at a density related to the quench rate of the control parameter.

The Kibble-Zurek mechanism (KZM) provides a theoretical framework that can predict the density of these defects or domain walls for a finite quench rate from universal properties of the continuous phase transition. First introduced by Kibble in the context of cosmology as a mechanism for the formation of cosmic strings in the early universe [1, 17], it was subsequently extended by Zurek to condensed matter systems [18–20]. It has since been successfully verified in many settings, including thermally driven transitions [21–25] and quantum phase transitions (QPTs) [26–28], and has been demonstrated to apply to quantum-annealing implementations of quantum computation [29, 30].

Recently, there has been increasing interest in studying first order QPTs [31–35], where metastability plays a crucial role, including in cold-atom systems [36–38]. A classical example of such metastability is the transition of supercooled water which remains liquid below the freezing point. For first-order quantum phase transitions, such ‘supercooling’ like behaviour can lead to a zero temperature false vacuum. This state plays an important role in particle physics and cosmology [39–41], but an understanding of how the metastable state decays is hampered by the lack of a general theoretical approach deal-

ing with first-order quantum phase transitions.

Here we propose an experimentally accessible nonequilibrium *first-order* QPT where the decay of such metastable states can be understood through the KZM. In particular, we study the persistence of the metastable state following a finite quench of the quadratic Zeeman shift in a spin-1 Bose-Einstein condensate (BEC) with ferromagnetic (FM) interactions. We demonstrate that the onset of decay of the metastable state representing the false vacuum agrees with the critical scaling law predicted by a generalisation of the KZM to our first order QPT.

A key feature of this phase transition in a ferromagnetic spinor BEC is the formation of phase-separated domains at long times past the transition point. Therefore, aside from the short time behaviour characterising the decay of the metastable state, we also apply the KZM to determine the scaling of the number of phase separated domains at latter times. In contrast to the short time behaviour, the KZM accurately predicts the scaling of the number of domains for intermediate quench rates whereas at very slow quenches, a scaling in agreement with Landau-Zener [27, 42] predictions emerges.

Focusing on an ultracold atomic system has the advantage that the QPT is easier to control for isolated systems. Atomic BECs in particular are pristine systems and offer a highly controllable platform where the strength of inter-atomic interactions and the confining trapping potentials can be tuned. Consequently, they are already popular example systems for phase-transition experiments [9, 43–45], as well as nonequilibrium physics, even in low dimensions, ranging from relaxation dynamics [46, 47] to quantum quenches [48–55]. Unlike scalar BECs, the spin degrees of freedom are not frozen out in spinor BECs. These additional degrees of freedom give rise to a non-trivial phase diagram even at zero temperature [56–61] and a correspondingly rich array of topological defects and textures [48, 56, 57, 62–66]. For these reasons, studying nonequilibrium QPTs with spinor BECs has attracted much attention [48, 52, 67–76].

In contrast to previous studies on QPTs, the first-order

QPT between the broken-axisymmetry (BA) phase and a ferromagnetic (FM) phase in a spin-1 BEC with FM interactions corresponds to a discontinuous quantum critical point (DQCP) [77], the quantum analogue of the classical discontinuous critical point [78, 79]. As it does not meet the general criteria of applicability of the standard KZ theory, the KZM has not hitherto been studied in this context. We consider, in particular, a one-dimensional (1D) spin-1 BEC with FM interactions in a ring-trap geometry. By quenching the quadratic Zeeman shift, the system can transition from the BA phase into a phase-separated FM phase where domains of atoms with opposite condensate-spin projection form [56]. Unlike the single-mode scenario in an antiferromagnetic condensate [80], where there is no domain formation, here phase separation is a consequence of the FM interactions under conservation of longitudinal magnetisation in a spatially extended BEC. Its 1D nature, however, has the advantage that once the domains form, they are frozen in and cannot undergo any coarsening dynamics [81, 82].

## II. RESULTS AND DISCUSSION

As our example system, we consider a spin-1 BEC described by the mean-field condensate spinor wave function  $\Psi = (\psi_1, \psi_0, \psi_{-1})^T$ . The Hamiltonian density then reads [56]

$$H = H_0 + \frac{c_0}{2}n^2 + \frac{c_1}{2}n^2|\langle\hat{\mathbf{F}}\rangle|^2 - pn\langle\hat{F}_z\rangle + qn\langle\hat{F}_z^2\rangle, \quad (1)$$

where  $H_0 = (\hbar^2/2M)|\nabla\Psi|^2 + nV(z)$  for atomic mass  $M$  and external trapping potential  $V(z)$ . Here,  $n = \sum_m \psi_m^* \psi_m$  is the total atomic density. The condensate spin operator  $\hat{\mathbf{F}} \equiv (\hat{F}_x, \hat{F}_y, \hat{F}_z)$  is the vector of spin-1 Pauli-type matrices such that  $\langle\hat{F}_\mu\rangle = \frac{1}{n} \sum_{mm'} \psi_m^* \langle\hat{F}_\mu\rangle_{mm'} \psi_{m'}$  for  $\mu = x, y, z$ . Conservation of angular momentum in  $s$ -wave scattering means that the longitudinal magnetisation  $M_z = \int\langle\hat{F}_z\rangle dz$  is conserved on experimental time scales. The spin-independent and -dependent interaction strengths arise from the  $s$ -wave scattering lengths  $a_{\mathcal{F}}$  in the spin- $\mathcal{F}$  channels of colliding spin-1 atoms as  $c_0 = 4\pi\hbar^2(a_0 + 2a_2)/3M$  and  $c_1 = 4\pi\hbar^2(a_2 - a_0)/3M$ , respectively. Linear and quadratic Zeeman shifts of strengths  $p$  and  $q$ , respectively, may arise from an applied magnetic field along the  $z$ -direction, or in the latter case be induced by an AC Stark shift [83, 84], which gives precise control over both strength and sign. Due to conservation of  $M_z$ , a uniform linear Zeeman shift only causes precession of the spin, under which the Hamiltonian is invariant. We therefore only consider effects from the quadratic Zeeman shift.

We consider atoms with  $c_1 < 0$ , such as  $^{87}\text{Rb}$  [85], which provides an interesting phase diagram arising from the competition between the third and last term in Eq. (1). A three-component BA phase with zero longitudinal magnetisation occurs for  $0 < Q = q/(|c_1|n_0) < 2$  [56] where  $n_0$  is the background density in a uniform system:

$$\psi_{\pm 1} = \frac{\sqrt{2n_0}}{4} \sqrt{2 - Q}, \quad \psi_0 = \frac{\sqrt{n_0}}{2} \sqrt{2 + Q}. \quad (2)$$

In addition, a FM state occurs for  $Q < 0$ :  $\Psi = (\sqrt{n_0}, 0, 0)^T$  or  $\Psi = (0, 0, \sqrt{n_0})^T$ . Since  $M_z$  is conserved, a BA initial condition with  $M_z = 0$  implies that the FM phase results in the formation of phase-separated domains with opposite spin projection as  $Q$  is ramped across the phase transition. The associated instability that leads to the emergence of phase separated domains when  $c_1 < 0$  is not captured in the single-mode approximation [60, 61].

Moreover, the transition point between the BA and FM phases at  $(q_c, p_c) = (0, 0)$  is a DQCP. Such a discontinuous phase transition satisfies five conditions [77], which permit scaling arguments to be applied. A critical point at  $q = q_c$  and  $p = p_c$ , where  $p$  functions as a symmetry-breaking field, is a DQCP of this kind if (1) the energy density  $\epsilon(q, p)$  across the transition is continuous,  $\epsilon(q_c^+, p_c) - \epsilon(q_c^-, p_c) = 0$ , but (2) its derivative is discontinuous,  $\partial\epsilon(q_c^+, p_c)/\partial q - \partial\epsilon(q_c^-, p_c)/\partial q \neq 0$ . Here,  $q_c^+$  and  $q_c^-$  correspond to approaching  $q_c$  from above or below, respectively. Further, (3) the order parameter  $m = -\partial\epsilon(q, p)/\partial p$  must exhibit a discontinuous jump with respect to  $q$  as the critical point is crossed,  $|m(q_c^-, p_c)| > |m(q_c^+, p_c)| = 0$ , and additionally, (4) the order parameter is also discontinuous with respect to  $p$ :  $|m(q_c, p_c^\pm)| > 0$ . Finally, we require (5) that the derivative of the energy be bounded as the critical point is approached:  $|\partial\epsilon(q_c^\pm, p_c)/\partial q| < \infty$ .

The energy densities per particle for the BA and FM states are, respectively [56],

$$\epsilon_{\text{BA}} = \frac{(-p^2 + q^2 + 2qc_1n_0)^2}{8c_1n_0q^2} + \frac{1}{2}c_0n_0, \quad (3)$$

$$\epsilon_{\text{FM}_\pm} = \mp p + q + \frac{1}{2}n_0(c_0 + c_1), \quad (4)$$

where the subscript  $+(-)$  denotes the FM phase with spin pointing up (down). These energies are continuous at the critical point  $(q_c, p_c) = (0, 0)$ . The derivatives, however, are discontinuous, but remain bounded. Meanwhile, the relevant order parameter for the BA and FM states is  $m_{\text{BA}} = p(p^2 - q^2 - 2qc_1n_0)/8c_1n_0q$  and  $m_{\text{FM}_\pm} = \pm 1$ , respectively, which is precisely the local magnetisation  $F_z = |\psi_1|^2 - |\psi_{-1}|^2$  in both phases [56]. For  $p_c = 0$  this order parameter is zero in the BA phase and becomes non-zero in the FM phase. A non-zero  $p$ , however, causes the order parameter to be non-zero in both phases. This means that the BA to FM transition satisfies all the conditions for a DQCP.

Next, we recall the key arguments in the KZM. A continuous second-order phase transition can be characterised by the divergence of an instantaneous correlation length  $\xi \sim |q(t) - q_c|^{-\nu}$  and an instantaneous relaxation time  $\tau \sim [\xi(t)]^z$ , where  $\nu$  and  $z$  are the correlation-length and dynamical critical exponents, respectively. In the standard QPT scenario, the relaxation time is set by the inverse of the energy gap  $\Delta$  between the ground state and the first excited state of a gapped mode [42, 67]:  $\tau \simeq \Delta^{-1}$ . A system initially prepared in the ground state follows this state adiabatically as long as the relaxation time remains small. However, as the critical point is approached, the energy gap vanishes and the relaxation time diverges, which leads to the breakdown of the adiabatic regime. This divides the dynamics into three stages: adiabatic, frozen, and adiabatic again as the system crosses the critical

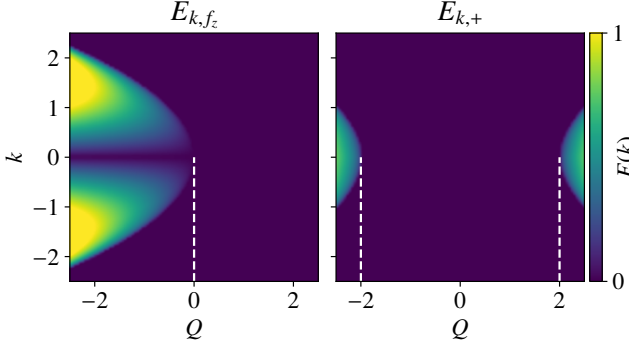


FIG. 1. Imaginary parts of  $E_{k,f_z}$  and  $E_{k,+}$ .  $E_{k,f_z}$  is unstable (positive imaginary part) for  $Q < 0$ , corresponding to the BA to FM QDCP, while  $E_{k,+}$  instead becomes unstable at the BA to polar second-order transition at  $Q = 2$ .

point. Assuming a quench of the form  $|q(t) - q_c| \sim |t/\tau_Q|$ , where  $\tau_Q^{-1}$  is the quench rate, the freezing time is estimated to be  $|\tilde{t}| = \tau(\tilde{t})$ . This leads to a scaling for the freezing time given by

$$|\tilde{t}| \sim \tau_Q^{zv/(zv+1)}. \quad (5)$$

It follows from this and the scaling of the correlation length that at the freezing time,  $\tilde{\xi} \sim \xi(\tilde{t}) \sim \tau_Q^{v/(zv+1)}$ . This provides an estimate for the density of defects or domains:  $N_d \sim \tilde{\xi}^{-d} \sim \tau_Q^{-dv/(zv+1)}$ .

Of the three Bogoliubov modes,  $E_{k,f_z}$  and  $E_{k,\pm}$ , for the BA phase [86] (see also Appendix), only  $E_{k,+}$  is gapped in the long-wavelength limit. This mode determines the scaling associated with the KZM for the transition from the polar to the BA phase [68]. By contrast, the relevant mode for the BA to FM transition is

$$E_{k,f_z}(k) = \sqrt{\epsilon_k(\epsilon_k + q)}, \quad (6)$$

where  $\epsilon_k = \hbar^2 k^2 / 2M$  is the kinetic energy. This spectrum is gapless in the long-wavelength limit. The imaginary part of  $E_{k,f_z}$  together with that of  $E_{k,+}$  is shown in Fig. 1 and clearly illustrates that an instability can occur at  $Q = 0$  only for modes with  $k \neq 0$ . These unstable modes are responsible for the formation of phase separated domains in the FM phase.

To derive a KZ scaling when the relevant mode is gapless, consider the more general spectrum,  $E_k^2 \sim |q(t) - q_c|^\alpha \epsilon_k^\eta + \epsilon_k^{2z}$ , of which Eq. (6) is a special case. To find scaling solutions consistent with the KZM where  $E_k \sim |q(t) - q_c|^\zeta$ , we make the ansatz  $k \sim |q(t) - q_c|^\nu$  (corresponding to  $k \sim \xi^{-1}$ ) and equate the two terms in the dispersion relation to derive the condition  $\alpha = \nu(2z - \eta)$ . For our gapless mode, the adiabatic-impulse approximation states that the impulse regime begins when  $E_k^2 = \dot{E}_k$ . This yields

$$|\tilde{t}| \sim \tau_Q^{\alpha/(2+\alpha)} \tilde{k}^{-\eta/(2+\alpha)} \sim \tau_Q^{\nu z/(1+\nu z)}, \quad (7)$$

for the freezing time upon using the above scaling assumed for  $k$ . This immediately implies the characteristic momen-

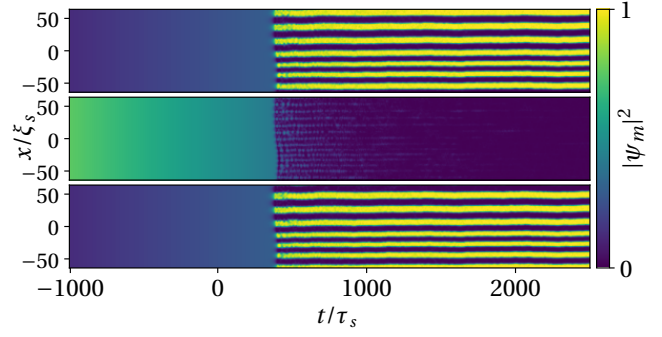


FIG. 2. Component densities in a  $64\xi_s$  subregion of the  $\psi_1$  (top),  $\psi_0$  (middle) and  $\psi_{-1}$  (bottom) components for a typical simulation with  $\tau_Q = 1000$ .

tum scale  $\tilde{k} \sim \tau_Q^{-\nu/(zv+1)}$  from which we extract the defect density where  $d$  is the dimensionality of the system (see also Appendix). Hence, the scaling relations of the KZM for a gapped mode is recovered for a gapless spectrum.

Specifically for our 1D system ( $d = 1$  and  $q_c = 0$ ), Eq. (6) implies  $\alpha = 1$ ,  $\eta = 2$  and  $z = 2$ . This is equivalent to setting  $z = 2$  and  $\nu = 1/2$  corresponding to a defect-density scaling

$$N_d \sim \tau_Q^{-1/4}. \quad (8)$$

Therefore, despite originating in the same model Hamiltonian, this scaling is clearly different from that reported for the KZM in continuous phase transitions through a QCP in spinor BECs [68, 70, 71, 73, 87]. Our results indicate a new scaling regime that is associated with the DQCP of this system.

To check our prediction, we numerically evolve the time-dependent spin-1 Gross-Pitaevskii equations (GPEs) obtained from Eq. (1) using a symplectic algorithm [88] (see Appendix). Typical results for  $\tau_Q = 1000$  are shown in Fig. 2. We see the clear formation of FM domains after crossing the critical point at  $t = 0$ . Figure 3 shows the normalised atom number for the  $\psi_0$  component as the system is quenched for various  $\tau_Q$ . Initially, the system tracks the BA-phase ground state [80], Eq. (2). After passing the critical point, the system is no longer able to adiabatically track the true ground state. Rather, it evolves in a metastable BA state, even for  $t/\tau_Q > 0$ , until it emerges from the impulse regime at a time clearly dependent on the quench rate. At this point, the metastable state decays with an associated abrupt drop in the density of the  $\psi_0$  component, signalling a discontinuous phase transition to the FM phase. This coincides with an increase in the  $\psi_{\pm 1}$  components, where the FM domains start to form (Fig. 3 inset).

To determine the freezing time as well as the short time scaling behaviour, we introduce  $\hat{a}_{k,\pm 1}$ , defined as the Fourier transforms of the  $\psi_{\pm 1}$  components, respectively. Since the transition to the FM phase results in phase-separated domains, driven by an instability associated with a Bogoliubov mode related to  $\hat{a}_{k,f_z} = (\hat{a}_{k,1} - \hat{a}_{k,-1})/\sqrt{2}$  (see Appendix), we extract the critical time  $\tilde{t}$  such that  $|\hat{a}_{k,f_z}(\tilde{t})| = 0.01 \times \max\{|\hat{a}_{k,f_z}(t)| : t\}$ . The critical Zeeman value is defined as  $Q_a = |Q(\tilde{t})|$ . The inset in Fig. 4 shows the typical growth of  $|\hat{a}_{k,f_z}|$ , which demonstrates that it remains zero until the system passes the critical point.

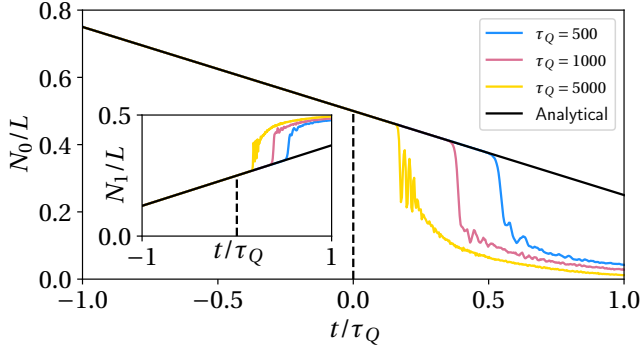


FIG. 3. Normalised atom number for the  $\psi_0$  component using the analytical prediction (black line) in Eq. (2). Also plotted are numerically calculated values for  $\tau_Q = 500, 1000, 5000$ . Inset: Normalised atom number for the  $\psi_1$  component using the same analytical and numerical data as the main figure. We note that  $N_1/L$  approaches 0.5 since the longitudinal magnetisation  $M_z = 0$  is conserved. The critical point is marked with a black dashed line.

Thereafter, it undergoes growth with strong oscillations. The choice of 0.01 when extracting  $\tilde{t}$  is arbitrary, but we find qualitatively similar results in tests with values up to 0.1.

Figure 4 reveals a clear  $Q_a \sim \tau_Q^{-1/2}$  power law for a large range of  $\tau_Q$ . Despite the discontinuous nature of the phase transition, scaling behaviour is still observed [89–91]. However, this scaling is different from that observed in numerical and experimental results concerning the continuous phase transitions in spin-1 BECs [68, 75]. The observed scaling is consistent with the Kibble-Zurek scaling presented above for our system. Taking  $\nu = 1/2$  and  $z = 2$ , and using Eq. (5), we obtain  $\tilde{t} \sim \tau_Q^{1/2}$ . Combining with the relation  $Q_a = |\tilde{t}/\tau_Q|$ , we also recover the  $Q_a \sim \tau_Q^{-1/2}$  scaling seen in our simulations.

To reinforce our conclusions, we recover the scaling laws by directly linearising the GP equations around the critical point. In this case, the temporal dependence of the quadratic Zeeman terms is treated directly. Following [68], we begin with a wave function close to the BA ground state,  $\Psi^T = (\psi_1 + \delta\psi_1(t), \psi_0 + \delta\psi_0(t), \psi_{-1} + \delta\psi_{-1}(t)) \exp(-i\mu t)$  where  $\psi_{\pm 1}, \psi_0$  are defined in Eq. (2) with  $Q = Q_0$ . Here,  $\mu = c_0 + c_1(2 - Q_0)/2$  is the chemical potential,  $0 \leq Q_0 \leq 2$  is a constant, and  $|\delta\psi_m(t)| \ll 1$ . The noise terms have to satisfy  $\int \sum_m \delta\psi_m + \delta\psi_m^* dz = 0$  to ensure the proper normalisation of the wave function and  $\int (\delta\psi_1 + \delta\psi_1^* + \delta\psi_{-1} + \delta\psi_{-1}^*) dz = 0$  to enforce conservation of magnetisation.

Linearizing the spin-1 GPEs about the state corresponding to  $Q = Q_0$  (see Appendix), we obtain

$$i\hbar \frac{d}{dt} G_y = \left[ -\frac{\hbar^2}{2M} \frac{d^2}{dz^2} - c_1 n_0 \left( Q - \frac{Q_0}{2} \right) \right] G_y - \frac{c_1 n_0 Q}{2} G_y^*, \quad (9)$$

where  $G_y = \delta\psi_1 - \delta\psi_{-1}$ . Next, we transform to momentum space and split  $G_y$  into real and imaginary parts, where  $a_y = \int \text{Re}(G_y) e^{ikz} dz$  and  $b_y = \int \text{Im}(G_y) e^{ikz} dz$ . We then solve for  $Q = -t/\tau_Q$ , by deriving the equation for  $d^2 a_y / dt^2$  across a DQCP. Rescaling time as  $t \rightarrow t\lambda$  with  $\lambda = \sqrt{\tau_s \tau_Q}$ , we arrive

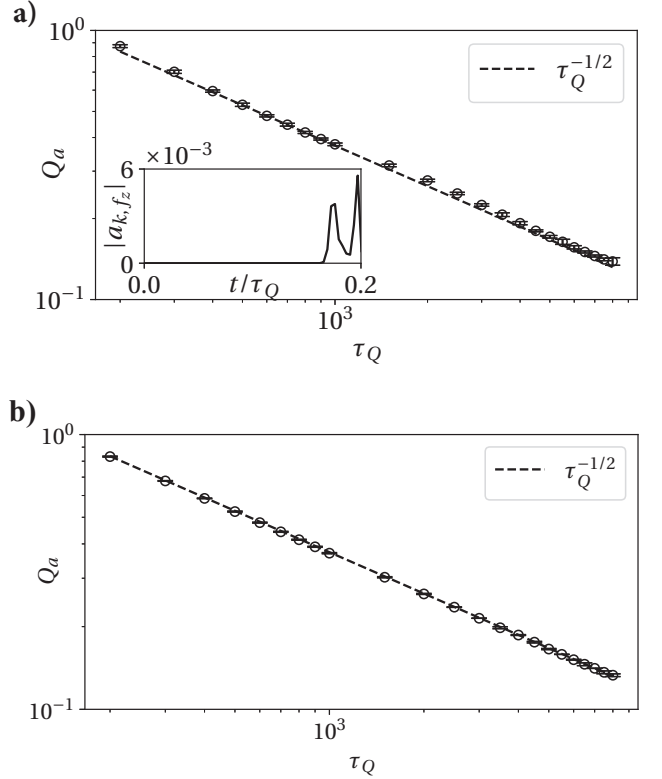


FIG. 4. **a)** Scaling of the critical value  $Q_a$  versus  $\tau_Q$ . Overlaid is the power-law scaling  $\tau_Q^{-1/2}$  (dashed line). Inset: the quantity  $|a_{k,f_z}|$  for  $\tau_Q = 5000$  and  $k = 1$ . **b)** Same but with  $Q_a$  calculated using the deviation from the analytically predicted value of  $\psi_0$  (see Appendix) reproducing the same scaling. For both methods, each point is averaged over 50 runs, and the error bars represent  $\pm 1$  standard deviation.

at

$$\frac{d^2 a_y}{dt^2} = \frac{-1}{(2\kappa^2 - t)} \frac{da_y}{dt} - \frac{1}{4} \left( \kappa^4 - 2\kappa^2 t + \frac{3t^2}{4} \right) a_y, \quad (10)$$

where  $\kappa^2 = \xi_s^2 k^2 \sqrt{\tau_Q / \tau_s}$ . This scaling ensures that the last term is independent of  $\tau_Q$ . The remaining dependence on  $\tau_Q$  is eliminated if we require that  $\kappa$  is constant, which implies  $k \sim \tau_Q^{-1/4}$ . Only under these conditions can we expect scaling solutions, and they are also consistent with the scaling of the correlation length and the dynamical exponents derived earlier based on the KZM.

The number of domains formed in the transition is a measurable quantity, which has been investigated in other works on the KZM [73, 81]. We numerically count the number of density peaks at the end of the simulation (Fig. 2). Fig. 5 shows the total number of FM domains for a broad range of  $\tau_Q$ . For sufficiently fast quenches ( $\tau_Q < 1000$ ), a clear power-law scaling  $N_d \sim \tau_Q^{-1/4}$  emerges, which agrees well with Eq. (8) as well as the scaling obtained with Eq. (10). As with  $\tilde{t}$ , the scaling for the DQCP is again different from that in analogous transitions across a continuous critical point [81].

Unlike  $Q_a$ , for slow quenches ( $\tau_Q > 1000$ ), there is a clear deviation from the predicted KZ scaling. Such differences in

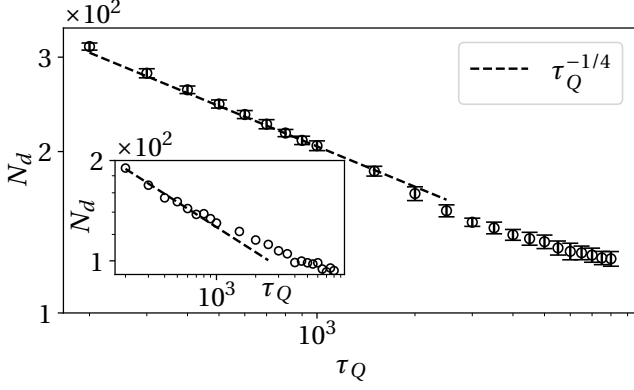


FIG. 5. The number of ferromagnetic domains as a function of the quench time,  $\tau_Q$ . Overlaid is the power-law scaling  $\tau_Q^{-1/4}$  (dashed line). Each point is averaged over 50 runs, and the error bars give  $\pm 1$  standard deviation. Inset: number of ferromagnetic domains in a quench that spans two phase transitions for the same quench times as the main figure.

the scaling of observables measured at much later times from the critical point have also been observed in [21, 73]. In our context, this deviation can be attributed to a cross-over into a different regime that follows predictions of a Landau-Zener model [27, 42, 92, 93].

Finally, we tested the robustness of the scaling by considering a quench that crosses two phase transitions. Starting from the polar state with  $Q = 2.5$ , we simulate a quench through the BA and then the FM states. Results are qualitatively similar (Fig. 5 inset), with a  $\tau_Q^{-1/4}$  scaling again emerging for the same range of  $\tau_Q$ , and with similar deviation for slow quenches.

In conclusion, we have shown that the KZM can be generalised to this discontinuous phase transition, leading to scaling laws that differ from those observed for phase transitions across continuous quantum critical points for the same spin-1 BEC model. We find excellent agreement with numerical simulation for both the short-time growth of the unstable excitations and the subsequent number of domains formed on longer time scales. Our results hold for experimentally accessible parameter regimes allowing these extensions of the KZM to be realized in current experiments on spinor BECs, which therefore emerge as prime candidates for testbed systems for investigating critical scaling in first-order quantum phase transitions, including as laboratory emulators for understanding false-vacuum decay [36–38, 94].

## ACKNOWLEDGMENTS

The numerical simulations were carried out on the High Performance Computing Cluster supported by the Research and Specialist Computing Support service at the University of East Anglia. MOB acknowledges support from EPSRC under grant number EP/V03832X/1.

## Appendix

### 1. Numerical Simulation.

We measure length and time in units of the spin healing length  $\xi_s = \hbar / \sqrt{2M|c_1|n_0}$  and the spin time  $\tau_s = \hbar/2|c_1|n_0$ , respectively. Our simulations are performed on a 1D grid of  $N_x = 16384$  points with a spacing of  $\Delta_x = 0.125\xi_s$ , considering a ring-shaped geometry by assuming periodic boundary conditions and  $V(z) = 0$ . We start from Eq. (2), adding small noise terms,  $\delta\psi_m$ , to each component, where  $|\delta\psi_m| \ll 1$ . The real and imaginary parts of  $\delta\psi_m$  are drawn from the probability distribution  $p(z) = \exp(-z^2/2\sigma^2)/(\sqrt{2\pi}\sigma)$ , with  $\sigma = 10^{-4}$  to remain close to the BA ground state. We vary the quadratic Zeeman shift as  $Q(t) = -t/\tau_Q$  for a range of quench times  $\tau_Q$ , starting at  $Q = 1$  and ending the simulation at  $Q = -2.5$ .

### 2. Bogoliubov modes for the broken-axisymmetry phase.

The broken-axisymmetry (BA) phase of a spin-1 BEC exhibits three Bogoliubov modes [86]. Here we rederive each mode explicitly from the relevant Bogoliubov transformations and explain why  $E_{\mathbf{k},f_z}$  is the relevant mode for the BA-to-ferromagnetic (FM) transition.

The broken-axisymmetry phase can be parameterised as

$$\zeta^{\text{BA}} = \left( \frac{\sin \theta}{\sqrt{2}}, \cos \theta, \frac{\sin \theta}{\sqrt{2}} \right), \quad (\text{A.1})$$

where  $\sin \theta = \sqrt{1/2 + q/(4nc_1)}$ . The fluctuation operators for this state are then defined as [86]:

$$\hat{a}_{\mathbf{k},d} = \frac{\sin \theta}{\sqrt{2}} (\hat{a}_{\mathbf{k},1} + \hat{a}_{\mathbf{k},-1}) + \cos \theta \hat{a}_{\mathbf{k},0}, \quad (\text{A.2})$$

$$\hat{a}_{\mathbf{k},f_z} = \frac{1}{\sqrt{2}} (\hat{a}_{\mathbf{k},1} - \hat{a}_{\mathbf{k},-1}), \quad (\text{A.3})$$

$$\hat{a}_{\mathbf{k},\theta} = \frac{\cos \theta}{\sqrt{2}} (\hat{a}_{\mathbf{k},1} + \hat{a}_{\mathbf{k},-1}) - \sin \theta \hat{a}_{\mathbf{k},0}, \quad (\text{A.4})$$

where on the right-hand side  $\hat{a}_{\mathbf{k},m}$  is the annihilation operator for a spin-1 boson in magnetic level  $m$  (for  $m = -1, 0, +1$ ), determined by expanding the wave-function field operator as

$$\hat{\psi}_m(\mathbf{x}) = \frac{1}{\sqrt{V}} \sum_{\mathbf{k}} \hat{a}_{\mathbf{k},m} e^{i\mathbf{k}\cdot\mathbf{x}}, \quad (\text{A.5})$$

where  $V$  is the volume of the system.

The sub-Hamiltonian for the spin fluctuation mode  $\hat{a}_{\mathbf{k},f_z}$  can be diagonalized using the transformation

$$\hat{b}_{\mathbf{k},f_z} = \sqrt{\frac{\epsilon_{\mathbf{k}} + q/2 + E_{\mathbf{k},f_z}}{2E_{\mathbf{k},f_z}}} \hat{a}_{\mathbf{k},f_z} + \sqrt{\frac{\epsilon_{\mathbf{k}} + q/2 - E_{\mathbf{k},f_z}}{2E_{\mathbf{k},f_z}}} \hat{a}_{-\mathbf{k},f_z}^\dagger, \quad (\text{A.6})$$

where  $\epsilon_{\mathbf{k}} = \hbar^2|\mathbf{k}|^2/2M$  is the kinetic energy and the Bogoliubov spectrum is given by

$$E_{\mathbf{k},f_z} = \sqrt{\epsilon_{\mathbf{k}}(\epsilon_{\mathbf{k}} + q)}. \quad (\text{A.7})$$

The sub-Hamiltonians for the density fluctuation mode  $\hat{a}_{\mathbf{k},d}$  and the  $\theta$  mode  $\hat{a}_{\mathbf{k},\theta}$  can be similarly diagonalized using opera-

tors  $\hat{b}_{\mathbf{k},+}$  and  $\hat{b}_{\mathbf{k},-}$ , which yields the remaining two Bogoliubov modes [86]:

$$E_{\mathbf{k},\pm} = \sqrt{\epsilon_{\mathbf{k}}^2 + n(c_0 - c_1)\epsilon_{\mathbf{k}} + 2(nc_1)^2(1 - \tilde{q}^2) \pm E_1(\mathbf{k})}, \quad (\text{A.8})$$

where  $\tilde{q} = -q/2c_1n$  and

$$E_1(\mathbf{k}) = \sqrt{[n(c_0 + 3c_1)\epsilon_{\mathbf{k}} + 2(c_1n)^2(1 - \tilde{q}^2)]^2 - 4c_1(c_0 + 2c_1)(n\tilde{q}\epsilon_{\mathbf{k}})^2}. \quad (\text{A.9})$$

The final, diagonalized Hamiltonian then reads

$$\hat{H}^{\text{BA}} = E_0^{\text{BA}} + \sum_{\mathbf{k} \neq 0} [E_{\mathbf{k},f_z} \hat{b}_{\mathbf{k},f_z}^\dagger \hat{b}_{\mathbf{k},f_z} + E_{\mathbf{k},-} \hat{b}_{\mathbf{k},-}^\dagger \hat{b}_{\mathbf{k},-} + E_{\mathbf{k},+} \hat{b}_{\mathbf{k},+}^\dagger \hat{b}_{\mathbf{k},+}], \quad (\text{A.10})$$

where  $E_0^{\text{BA}}$  is the ground state energy for the BA phase, which is explicitly derived in Ref. [86].

We now consider our 1D system. In the long-wavelength limit,  $k \rightarrow 0$ , the only non-zero (gapped) mode is  $E_{k,+} = \sqrt{4(c_1n)^2(1 - \tilde{q}^2)}$  which has the form  $E_{k,+} \sim \sqrt{q_c'^2 - q^2}$  with  $q_c' = 2c_1n$ . The relevant mode of the BA to FM transition is found from the imaginary parts of the Bogoliubov energies (Fig 1). For  $|Q| > 2$ , where  $Q \equiv q/(|c_1|n)$ ,  $E_{k,+}$  has a positive imaginary part, indicating instability. The critical point  $Q = 2$  ( $q = q_c'$ ) corresponds to the second-order transition between the polar and BA phases, for which  $E_{k,+}$  therefore is the corresponding Bogoliubov energy.

However, for  $Q < 0$  the imaginary part of  $E_{k,f_z}$  mode becomes non-zero and positive, and thus unstable. This corresponds precisely to the transition from the BA to the FM phase at  $Q = 0$  that we are interested in here, and therefore  $E_{k,f_z}$  is the relevant mode to study. Note that the  $E_{k,f_z}$  mode does not give rise to instability at  $k = 0$ . Therefore, studies focusing on this mode at  $k = 0$  only do not capture the phase transition that occurs at  $Q = 0$  [60, 61, 80]. In contrast, the  $k = 0$  mode corresponds to the most unstable mode for  $E_{k,+}$ , and thus it suffices to choose this Bogoliubov energy to capture the phase transition that occurs at  $Q = 2$ . In practice, the  $Q = -2$  transition is not realized since the instability of  $E_{k,f_z}$  at any  $k \neq 0$  will typically arise at  $Q = 0$  when  $Q$  is quenched from positive to negative values.

### 3. Scaling of Density of Defects from the Kibble-Zurek Mechanism.

Given the form of our dispersion relation together with the scaling relation for the relaxation time provided by the KZM, which assumes  $\tau \sim \xi^z$ , we will consider a dispersion relation of the general form [77]

$$\omega^2 \sim |q - q_c|^\alpha k^\eta + k^{2z} \quad (\text{A.11})$$

for a critical point at  $q = q_c$ . For a scaling solution to arise that is consistent with the scaling of the relaxation time, we require  $\omega \sim k^z$  with  $k \sim \xi^{-1} \sim |q - q_c|^\nu$ . Combining these relations, Eq. (A.11) implies that

$$\alpha = \nu(2z - \eta). \quad (\text{A.12})$$

In our system  $q_c = 0$  and  $q = -t/\tau_Q$ . Therefore, Eq. (A.11) simplifies to

$$\omega^2 \sim \frac{|t|^\alpha}{\tau_Q^\alpha} k^\eta. \quad (\text{A.13})$$

Now let us consider the adiabatic-impulse approximation for a gapped spectrum, with an energy gap given by  $\Delta(t)$ . In this case,  $\tau \sim 1/\Delta$  and so far from the critical point where  $\Delta$  is large, the relaxation time is small and the evolution is adiabatic, meaning that the system is able to adjust quickly enough and can therefore track the true ground state of the system. As the critical point is approached,  $\Delta$  vanishes and the relaxation time diverges. At some instant  $\tilde{t}$ , the reaction time becomes comparable to the transition time,  $\Delta/\dot{\Delta}$  and the system is no longer able to adiabatically track the evolution. This point is the onset of the impulse regime, where the state becomes frozen. The freezing time is therefore often evaluated from the condition

$$\frac{1}{\Delta(\tilde{t})} \sim \frac{\Delta(\tilde{t})}{\dot{\Delta}(\tilde{t})}. \quad (\text{A.14})$$

For a gapless spectrum, which is the case for the BA-to-FM transition, we work with the form of the dispersion relation as given by Eq. (A.13) and determine the onset of the impulse regime with the condition  $\omega^2 = \dot{\omega}$ . This yields

$$\frac{\alpha}{2\tau_Q^{\alpha/2}} |\tilde{t}|^{\alpha(\alpha/2-1)} \tilde{k}^{\eta/2} \sim \frac{|\tilde{t}|^\alpha}{\tau_Q^\alpha} \tilde{k}^\eta, \quad (\text{A.15})$$

which leads us directly to the scaling relation for the freezing time

$$|\tilde{t}| \sim \tau_Q^{\alpha/(2+\alpha)} \tilde{k}^{-\eta/(2+\alpha)}. \quad (\text{A.16})$$

To obtain the characteristic momentum scale, we substitute Eq. (A.16) back into Eq. (A.15), which yields

$$\tilde{k} \sim \tau_Q^{\alpha/(\eta-(2+\alpha)z)}. \quad (\text{A.17})$$

#### 4. Extracting the freezing time

In order to extract the freezing time  $\tilde{t}$  of the system, an appropriate quantity must be chosen. Since the transition to the FM phase causes the formation of phase-separated domains, a natural choice is to measure fluctuations in the difference of the populations of  $\psi_{\pm 1}$  [86]. To do this, we first construct the Fourier transforms of the  $\psi_{\pm 1}$  components as  $\hat{a}_{\pm 1}(k) = \int \psi_{\pm 1} e^{-2\pi i k \cdot x} dx$ . After passing through the critical point into the FM phase, the difference  $\hat{a}_{k,f_z}(k) = \hat{a}_1(k) - \hat{a}_{-1}(k) / \sqrt{2}$  generates measurable fluctuations as FM domains with opposite spin start to form [see inset of Fig. 4(a)], while before the transition it remains zero (due to the absence of domains). To measure the freezing time, we extract the time at which  $|\hat{a}_{k,f_z}(k)|$  exceeds some appropriately chosen value. In our numerical simulations, we take this value to be 1% of the maximum value of  $|\hat{a}_{k,f_z}(k)|$  over the entire simulation.

An alternative choice is the population of the  $\psi_0$  component. Here, instead of measuring the growth of a quantity, we now extract the freezing time as the time required for the  $\psi_0$

component to deviate from its analytically calculated value in the (metastable) BA phase  $\psi_0 = \sqrt{2 + Q}/2$  (Fig. 3). In particular, we choose the freezing time to be the time at which the deviation reaches 1% of the analytically predicted value, yielding Fig. 4(b). We see that, despite using an entirely different quantity to measure the freezing time, the resulting scaling of  $Q_a$  is the same as when calculated from  $|\hat{a}_{k,f_z}(k)|$ .

#### 5. Deriving scaling near the critical point.

The spin-1 Gross-Pitaevskii equations (GPEs) are given as [56]:

$$i\hbar \frac{\partial \Psi}{\partial t} = \left[ -\frac{\hbar^2 \nabla^2}{2M} - p\hat{F}_z + q\hat{F}_z^2 + c_0 n + c_1 n(\hat{\mathbf{F}}) \cdot \hat{\mathbf{F}} \right] \Psi. \quad (\text{A.18})$$

Recall that we start from a BA phase of the form  $\Psi^T = (\psi_1 + \delta\psi_1(t), \psi_0 + \delta\psi_0(t), \psi_{-1} + \delta\psi_{-1}(t)) \exp(-i\mu t)$ . Substituting this expression into the GPEs and keeping leading order terms in  $\delta\psi_m$  yields the following equations for  $\delta\psi_{\pm 1}$  ( $p = 0$ )

$$i\hbar \frac{\partial \delta\psi_1}{\partial t} = \left[ -\frac{\hbar^2}{2M} \frac{d^2}{dz^2} + q - \mu + \frac{n_0(10c_0 + 6c_1 - (c_0 - c_2)Q)}{8} \right] \delta\psi_1 + \frac{n_0 \sqrt{2(4 - Q^2)}}{8} [(c_0 + 3c_1)\delta\psi_0 + (c_0 + c_1)\delta\psi_0^*] + \frac{n_0(2 - Q)}{8} [(c_0 - c_1)\delta\psi_{-1} + (c_0 + c_1)\delta\psi_1^*] + \frac{n_0}{8} [(2 - Q)c_0 + (2 + 3Q)c_1] \delta\psi_{-1}^*, \quad (\text{A.19})$$

$$i\hbar \frac{\partial \delta\psi_{-1}}{\partial t} = \left[ -\frac{\hbar^2}{2M} \frac{d^2}{dz^2} + q - \mu + \frac{n_0(10c_0 + 6c_1 - (c_0 - c_2)Q)}{8} \right] \delta\psi_{-1} + \frac{n_0 \sqrt{2(4 - Q^2)}}{8} [(c_0 + 3c_1)\delta\psi_0 + (c_0 + c_1)\delta\psi_0^*] + \frac{n_0(2 - Q)}{8} [(c_0 - c_1)\delta\psi_1 + (c_0 + c_1)\delta\psi_{-1}^*] + \frac{n_0}{8} [(2 - Q)c_0 + (2 + 3Q)c_1] \delta\psi_1^*. \quad (\text{A.20})$$

Subtracting Eq. (A.20) from Eq. (A.19) results in the differential equation for  $G_y = \delta\psi_1 - \delta\psi_{-1}$ :

$$i\hbar \frac{dG_y}{dt} = \left[ -\frac{\hbar^2}{2M} \frac{d^2}{dz^2} + q - \mu + n_0(c_0 + c_1) \right] G_y - \frac{c_1 n_0 Q}{2} G_y^*. \quad (\text{A.21})$$

Additionally, to calculate the chemical potential, we take the  $\psi_0$  component of Eq. (A.18) keeping lead order terms and assuming a stationary state, which leads to  $\mu = c_0 n_0 + c_1 n_0(2 - Q_0)/2$  where  $Q_0$  is a constant. Substituting this expression and  $q(t) = -c_1 n_0 Q(t)$  into Eq. (A.21) yields

$$i\hbar \frac{dG_y}{dt} = \left[ -\frac{\hbar^2}{2M} \frac{d^2}{dz^2} - c_1 n_0 \left( Q - \frac{Q_0}{2} \right) \right] G_y - \frac{c_1 n_0 Q}{2} G_y^*. \quad (\text{A.22})$$

To progress, we split  $G_y$  into real and imaginary parts and take the Fourier transform:  $a_y = \int \text{Re}(G_y) e^{ikz} dz$  and  $b_y = \int \text{Im}(G_y) e^{ikz} dz$ . Substituting into Eq. (A.22) yields the matrix equation

$$\frac{d}{dt} \begin{bmatrix} a_y \\ b_y \end{bmatrix} = \begin{pmatrix} 0 & \frac{\hbar k^2}{2M} - \frac{c_1 n_0}{2\hbar} (Q - Q_0) \\ \frac{c_1 n_0}{2\hbar} (3Q - Q_0) - \frac{\hbar k^2}{2M} & 0 \end{pmatrix} \begin{bmatrix} a_y \\ b_y \end{bmatrix}. \quad (\text{A.23})$$

To solve the above equation, we construct the equation for  $\frac{d^2 a_y}{dt^2}$  and take  $Q_0 = 0$ , which yields

$$\frac{d^2 a_y}{dt^2} = \frac{c_1 n_0}{2\hbar \tau_Q} b_y + \left( \frac{\hbar^2 k^2}{2M} - \frac{c_1 n_0 Q}{2\hbar} \right) \frac{db_y}{dt}. \quad (\text{A.24})$$

Expressions for  $b_y$  and  $db_y/dt$  are found from Eq. (A.23). Substituting these in yields the following equation for  $d^2a_y/dt^2$ :

$$\frac{d^2a_y}{dt^2} = \frac{1}{\tau_Q \left( \frac{\hbar^2 k^2}{Mc_1 n_0} - Q \right)} \frac{da_y}{dt} - \left( \frac{\hbar^2 k^4}{4M^2} - \frac{k^2 c_1 n_0 Q}{M} + \frac{3c_1^2 n_0^2 Q^2}{4\hbar^2} \right) a_y. \quad (\text{A.25})$$

To simplify the above expression, we use the spin healing length  $\xi_s = \hbar / \sqrt{2|c_1|n_0}$  and the spin time  $\tau_s = \hbar / |c_1|n_0$ :

$$\frac{d^2a_y}{dt^2} = \frac{-1}{(2\xi_s^2 k^2 \tau_Q - t)} \frac{da_y}{dt} - \left( \frac{\xi_s^4 k^4}{4\tau_s^2} - \frac{\xi_s^2 k^2 t}{2\tau_s^2 \tau_Q} + \frac{3t^2}{16\tau_s^2 \tau_Q^2} \right) a_y. \quad (\text{A.26})$$

Rescaling time as  $t \rightarrow t\lambda$  with  $\lambda = \sqrt{\tau_s \tau_Q}$ , leads to the differential equation

$$\frac{d^2a_y}{dt^2} = \frac{-1}{(2\kappa^2 - t)} \frac{da_y}{dt} - \frac{1}{4} \left( \kappa^4 - 2\kappa^2 t + \frac{3t^2}{4} \right) a_y, \quad (\text{A.27})$$

where  $\kappa^2 = \xi_s^2 k^2 \sqrt{\tau_Q / \tau_s}$ .

- 
- [1] T. W. Kibble, *Phys. Rep.* **67**, 183 (1980).  
[2] A. Mazumdar and G. White, *Rep. Prog. Phys.* **82**, 076901 (2019).  
[3] I. Chuang, R. Durrer, N. Turok, and B. Yurke, *Science* **251**, 1336 (1991).  
[4] P. C. Hendry, N. S. Lawson, R. A. Lee, P. V. McClintock, and C. D. Williams, *Nature* **368**, 315 (1994).  
[5] C. Bäuerle, Y. M. Bunkov, S. N. Fisher, H. Godfrin, and G. R. Pickett, *Nature* **382**, 332 (1996).  
[6] V. M. H. Ruutu, V. B. Eltsov, A. J. Gill, T. W. B. Kibble, M. Krusius, Y. G. Makhlin, B. Plaçais, G. E. Volovik, and W. Xu, *Nature* **382**, 334 (1996).  
[7] S. L. Sondhi, S. M. Girvin, J. P. Carini, and D. Shahar, *Rev. Mod. Phys.* **69**, 315 (1997).  
[8] A. Polkovnikov, K. Sengupta, A. Silva, and M. Vengalattore, *Rev. Mod. Phys.* **83**, 863 (2011).  
[9] Z. Hadzibabic, P. Krüger, M. Cheneau, B. Battelier, and J. Dalibard, *Nature* **441**, 1118 (2006).  
[10] T. Langen, R. Geiger, and J. Schmiedmayer, *Annu. Rev. Condens. Matter Phys.* **6**, 201 (2015).  
[11] R. J. Fletcher, M. Robert-de-Saint-Vincent, J. Man, N. Navon, R. P. Smith, K. G. H. Viebahn, and Z. Hadzibabic, *Phys. Rev. Lett.* **114**, 255302 (2015).  
[12] I.-K. Liu, S. Donadello, G. Lamporesi, G. Ferrari, S.-C. Gou, F. Dalfovo, and N. P. Proukakis, *Commun. Phys.* **1**, 24 (2018).  
[13] P. C. Hohenberg and B. I. Halperin, *Rev. Mod. Phys.* **49**, 435 (1977).  
[14] N. Goldenfeld, *Lectures on Phase Transitions and the Renormalization Group* (CRC Press, 1992).  
[15] J. Dziarmaga, *Adv. Phys.* **59**, 1063 (2010).  
[16] A. Del Campo and W. H. Zurek, *Int. J. Mod. Phys. A* **29**, 1430018 (2014).  
[17] T. W. Kibble, *J. Phys. Math. Gen.* **9**, 1387 (1976).  
[18] W. H. Zurek, *Nature* **317**, 505 (1985).  
[19] W. Zurek, *Acta Phys. Pol. B* **24**, 1301 (1993).  
[20] W. H. Zurek, *Phys. Rep.* **276**, 177 (1996).  
[21] S.-W. Su, S.-C. Gou, A. Bradley, O. Fialko, and J. Brand, *Phys. Rev. Lett.* **110**, 215302 (2013).  
[22] G. Lamporesi, S. Donadello, S. Serafini, F. Dalfovo, and G. Ferrari, *Nat. Phys.* **9**, 656 (2013).  
[23] C.-W. Liu, A. Polkovnikov, and A. W. Sandvik, *Phys. Rev. B* **89**, 054307 (2014).  
[24] S. Donadello, S. Serafini, T. Bienaimé, F. Dalfovo, G. Lamporesi, and G. Ferrari, *Phys. Rev. A* **94**, 023628 (2016).  
[25] J. Beugnon and N. Navon, *J. Phys. B: At. Mol. Opt. Phys.* **50**, 022002 (2017).  
[26] J. Dziarmaga, *Phys. Rev. Lett.* **95**, 245701 (2005).  
[27] B. Damski, *Phys. Rev. Lett.* **95**, 035701 (2005).  
[28] C.-R. Yi, S. Liu, R.-H. Jiao, J.-Y. Zhang, Y.-S. Zhang, and S. Chen, *Phys. Rev. Lett.* **125**, 260603 (2020).  
[29] A. D. King, S. Suzuki, J. Raymond, A. Zucca, T. Lanting, F. Altomare, A. J. Berkley, S. Ejtemaee, E. Hoskinson, S. Huang, E. Ladizinsky, A. J. R. MacDonald, G. Marsden, T. Oh, G. Poulin-Lamarre, M. Reis, C. Rich, Y. Sato, J. D. Whittaker, J. Yao, R. Harris, D. A. Lidar, H. Nishimori, and M. H. Amin, *Nat. Phys.* **18**, 1324 (2022).  
[30] A. D. King, J. Raymond, T. Lanting, R. Harris, A. Zucca, F. Altomare, A. J. Berkley, K. Boothby, S. Ejtemaee, C. Enderud, E. Hoskinson, S. Huang, E. Ladizinsky, A. J. R. MacDonald, G. Marsden, R. Molavi, T. Oh, G. Poulin-Lamarre, M. Reis, C. Rich, Y. Sato, N. Tsai, M. Volkmann, J. D. Whittaker, J. Yao, A. W. Sandvik, and M. H. Amin, *Nature* **617**, 61 (2023).  
[31] I. B. Coulamy, A. Saguia, and M. S. Sarandy, *Phys. Rev. E* **95**, 022127 (2017).  
[32] K. Shimizu, T. Hirano, J. Park, Y. Kuno, and I. Ichinose, *New J. Phys.* **20**, 083006 (2018).  
[33] A. Pelissetto, D. Rossini, and E. Vicari, *Phys. Rev. E* **97**, 052148 (2018).  
[34] A. Pelissetto, D. Rossini, and E. Vicari, *Phys. Rev. E* **102**, 012143 (2020).  
[35] A. Sinha, T. Chanda, and J. Dziarmaga, *Phys. Rev. B* **103**, L220302 (2021).  
[36] T. P. Billam, K. Brown, and I. G. Moss, *Phys. Rev. A* **105**, L041301 (2022).  
[37] B. Song, S. Dutta, S. Bhave, J.-C. Yu, E. Carter, N. Cooper, and U. Schneider, *Nat. Phys.* **18**, 259 (2022).  
[38] A. Zenesini, A. Berti, R. Cominotti, C. Rogora, I. G. Moss, T. P. Billam, I. Carusotto, G. Lamporesi, A. Recati, and G. Ferrari,



- Observation of false vacuum decay via bubble formation in ferromagnetic superfluids, [arXiv:2305.05225 \[hep-ph\]](https://arxiv.org/abs/2305.05225).
- [39] S. Coleman, *Phys. Rev. D* **15**, 2929 (1977).
- [40] O. Fialko, B. Opanchuk, A. I. Sidorov, P. D. Drummond, and J. Brand, *Europhys. Lett.* **110**, 56001 (2015).
- [41] F. Devoto, S. Devoto, L. D. Luzio, and G. Ridolfi, *J. Phys. G: Nucl. Part. Phys.* **49**, 103001 (2022).
- [42] W. H. Zurek, U. Dörner, and P. Zoller, *Phys. Rev. Lett.* **95**, 105701 (2005).
- [43] P. Krüger, Z. Hadzibabic, and J. Dalibard, *Phys. Rev. Lett.* **99**, 040402 (2007).
- [44] C. N. Weiler, T. W. Neely, D. R. Scherer, A. S. Bradley, M. J. Davis, and B. P. Anderson, *Nature* **455**, 948 (2008).
- [45] L. Chomaz, L. Corman, T. Bienaimé, R. Desbuquois, C. Weitenberg, S. Nascimbène, J. Beugnon, and J. Dalibard, *Nat. Commun.* **6**, 6162 (2015).
- [46] M. Gring, M. Kuhnert, T. Langen, T. Kitagawa, B. Rauer, M. Schreitl, I. Mazets, D. A. Smith, E. Demler, and J. Schmiedmayer, *Science* **337**, 1318 (2012).
- [47] M. T. Reeves, K. Goddard-Lee, G. Gauthier, O. R. Stockdale, H. Salman, T. Edmonds, X. Yu, A. S. Bradley, M. Baker, H. Rubinsztein-Dunlop, M. J. Davis, and T. W. Neely, *Phys. Rev. X* **12**, 011031 (2022).
- [48] L. E. Sadler, J. M. Higbie, S. R. Leslie, M. Vengalattore, and D. M. Stamper-Kurn, *Nature* **443**, 312 (2006).
- [49] R. Barnett, A. Polkovnikov, and M. Vengalattore, *Phys. Rev. A* **84**, 023606 (2011).
- [50] N. Navon, A. L. Gaunt, R. P. Smith, and Z. Hadzibabic, *Science* **347**, 167 (2015).
- [51] L. M. Symes and P. B. Blakie, *Phys. Rev. E* **95**, 013311 (2017).
- [52] S. Kang, S. W. Seo, J. H. Kim, and Y. Shin, *Phys. Rev. A* **95**, 053638 (2017).
- [53] M. Prüfer, P. Kunkel, H. Strobel, S. Lannig, D. Linnemann, C. M. Schmied, J. Berges, T. Gasenzer, and M. K. Oberthaler, *Nature* **563**, 217 (2018).
- [54] C.-M. Schmied, T. Gasenzer, and P. B. Blakie, *Phys. Rev. A* **100**, 033603 (2019).
- [55] I.-K. Liu, J. Dziarmaga, S.-C. Gou, F. Dalfovo, and N. P. Proukakis, *Phys. Rev. Res.* **2**, 033183 (2020).
- [56] Y. Kawaguchi and M. Ueda, *Phys. Rep.* **520**, 253 (2012).
- [57] D. M. Stamper-Kurn and M. Ueda, *Rev. Mod. Phys.* **85**, 1191 (2013).
- [58] K. Murata, H. Saito, and M. Ueda, *Phys. Rev. A* **75**, 013607 (2007).
- [59] M. O. Borgh, J. Lovegrove, and J. Ruostekoski, *New J. Phys.* **16**, 053046 (2014).
- [60] M. Matuszewski, T. J. Alexander, and Y. S. Kivshar, *Phys. Rev. A* **80**, 023602 (2009).
- [61] S. S. Mirkhalaf, D. Benedicto Orenes, M. W. Mitchell, and E. Witkowska, *Phys. Rev. A* **103**, 023317 (2021).
- [62] A. E. Leanhardt, Y. Shin, D. Kielpinski, D. E. Pritchard, and W. Ketterle, *Phys. Rev. Lett.* **90**, 140403 (2003).
- [63] S. W. Seo, S. Kang, W. J. Kwon, and Y. I. Shin, *Phys. Rev. Lett.* **115**, 015301 (2015).
- [64] S. Kang, S. W. Seo, H. Takeuchi, and Y. Shin, *Phys. Rev. Lett.* **122**, 095301 (2019).
- [65] L. S. Weiss, M. O. Borgh, A. Blinova, T. Ollikainen, M. Möttönen, J. Ruostekoski, and D. S. Hall, *Nat. Commun.* **10**, 4772 (2019).
- [66] Y. Xiao, M. O. Borgh, A. Blinova, T. Ollikainen, J. Ruostekoski, and D. S. Hall, *Nat. Commun.* **13**, 4635 (2022).
- [67] B. Damski and W. H. Zurek, *Phys. Rev. A* **73**, 063405 (2006).
- [68] B. Damski and W. H. Zurek, *Phys. Rev. Lett.* **99**, 130402 (2007).
- [69] A. Lamacraft, *Phys. Rev. Lett.* **98**, 160404 (2007).
- [70] H. Saito, Y. Kawaguchi, and M. Ueda, *Phys. Rev. A* **75**, 013621 (2007).
- [71] H. Saito, Y. Kawaguchi, and M. Ueda, *Phys. Rev. A* **76**, 043613 (2007).
- [72] M. Vengalattore, S. R. Leslie, J. Guzman, and D. M. Stamper-Kurn, *Phys. Rev. Lett.* **100**, 170403 (2008).
- [73] T. Świsłocki, E. Witkowska, J. Dziarmaga, and M. Matuszewski, *Phys. Rev. Lett.* **110**, 045303 (2013).
- [74] E. Witkowska, J. Dziarmaga, T. Świsłocki, and M. Matuszewski, *Phys. Rev. B* **88**, 054508 (2013).
- [75] M. Anquez, B. A. Robbins, H. M. Bharath, M. Boguslawski, T. M. Hoang, and M. S. Chapman, *Phys. Rev. Lett.* **116**, 155301 (2016).
- [76] L. A. Williamson and P. B. Blakie, *Phys. Rev. A* **94**, 063615 (2016).
- [77] S. Suzuki and A. Dutta, *Phys. Rev. B* **92**, 064419 (2015).
- [78] M. Nauenberg, *J. Phys. A: Math. Gen.* **8**, 925 (1975).
- [79] M. E. Fisher and A. N. Berker, *Phys. Rev. B* **26**, 2507 (1982).
- [80] L.-Y. Qiu, H.-Y. Liang, Y.-B. Yang, H.-X. Yang, T. Tian, Y. Xu, and L.-M. Duan, *Sci. Adv.* **6**, eaba7292 (2020).
- [81] J. Sabbatini, W. H. Zurek, and M. J. Davis, *Phys. Rev. Lett.* **107**, 230402 (2011).
- [82] J. Sabbatini, W. H. Zurek, and M. J. Davis, *New J. Phys.* **14**, 095030 (2012).
- [83] F. Gerbier, A. Widera, S. Fölling, O. Mandel, and I. Bloch, *Phys. Rev. A* **73**, 041602(R) (2006).
- [84] L. Santos, M. Fattori, J. Stuhler, and T. Pfau, *Phys. Rev. A* **75**, 053606 (2007).
- [85] N. N. Klausen, J. L. Bohn, and C. H. Greene, *Phys. Rev. A* **64**, 053602 (2001).
- [86] S. Uchino, M. Kobayashi, and M. Ueda, *Phys. Rev. A* **81**, 063632 (2010).
- [87] H. Saito, Y. Kawaguchi, and M. Ueda, *J. Phys. Condens. Matter* **25**, 404212 (2013).
- [88] L. M. Symes, R. I. McLachlan, and P. B. Blakie, *Phys. Rev. E* **93**, 053309 (2016).
- [89] L. Turban and F. Iglói, *Phys. Rev. B* **66**, 014440 (2002).
- [90] M. A. Continentino and A. S. Ferreira, *Phys. Stat. Mech. Its Appl.* **339**, 461 (2004).
- [91] M. Continentino, *Quantum Scaling in Many-Body Systems: An Approach to Quantum Phase Transitions*, 2nd ed. (Cambridge University Press, Cambridge, 2017).
- [92] F. Pellegrini, S. Montangero, G. E. Santoro, and R. Fazio, *Phys. Rev. B* **77**, 140404(R) (2008).
- [93] U. Divakaran, A. Dutta, and D. Sen, *Phys. Rev. B* **78**, 144301 (2008).
- [94] G. Lagnese, F. M. Surace, S. Morampudi, and F. Wilczek, Detecting a long lived false vacuum with quantum quenches, [arXiv:2308.08340 \[cond-mat.stat-mech\]](https://arxiv.org/abs/2308.08340).